Quantitative Analysis of Redox-Inactive Ions by AC Voltammetry at a Polarised Interface between Two Immiscible Electrolyte Solutions

Marco F. Suárez-Herrera[a]* and Micheál D. Scanlon[b]*

[a] Departamento De Química, Facultad De Ciencias, Universidad Nacional De Colombia, Cra 30 # 45-03, Edificio 451, Bogotá, Colombia.

[b] The Bernal Institute and Department of Chemical Sciences, School of Natural Sciences, University of Limerick (UL), Limerick V94 T9PX, Ireland.

Corresponding Authors

*Marco F. Suárez-Herrera. E-mail: mfsuarezh@unal.edu.co

*Micheál D. Scanlon. E-mail: micheal.scanlon@ul.ie

Abstract

The interface between two immiscible electrolyte solutions (ITIES) is ideally suited to detect redox-inactive ions by their ion transfer. Such electroanalysis, based on the Nernst-Donnan equation, has been predominantly carried out by amperometry, cyclic or differential pulse voltammetry. Here, we introduce a new electroanalytical method based on AC voltammetry with inherent advantages over traditional approaches such as avoidance of positive feedback *iR* compensation, a major issue for liquid|liquid electrochemical cells containing resistive organic media and interfacial areas in the cm^2 and mm^2 range. A theoretical background outlining the generation of the analytical signal is provided and based on extracting the component that depends on the Warburg impedance from the total impedance. The quantitative detection of a series of model redox-inactive tetraalkylammonium cations is demonstrated, with evidence provided of the transient adsorption of these cations at the interface during the course of ion transfer. As ion transfer is diffusion limited, by changing the voltage excitation frequency during AC voltammetry, the intensity of the Faradaic response can be enhanced at low frequencies (1 Hz) or made to disappear completely at higher frequencies (99 Hz). The latter produces an AC voltammogram equivalent to a "blank" measurement in the absence of analyte and is ideal for background subtraction. Major opportunities therefore exist for the sensitive detection of ionic analyte when a "blank" measurement in the absence of analyte is impossible. This approach is particularly useful to deconvolute signals related to reversible

electrochemical reactions from those due to irreversible processes, which do not give AC signals.

Introduction

The trace analysis of redox-inactive ions impacts a broad range of fields including biomedical diagnostics,[1,2] environmental monitoring,[3,4] and the agricultural industry.[5] Electroanalytical methods have the advantages of ease of miniaturisation and device portability for on-site analysis, relatively low-cost per analysis, short response times, and high sensitivity. Electrochemistry at an interface between two immiscible electrolyte solutions (ITIES) is ideally suited to detect ions through the generation of an electroanalytical signal by transfer of the ionic species across a polarised aqueous|organic (w|o) interface.[6,7] Ion transfer is initiated by changing the relative interfacial concentrations of the ion, *i*, on either side of the w|o interface $\left(c^{\mathrm{o}}_{i,x=0}/c^{\mathrm{w}}_{i,x=0}\right)$ upon external manipulation of the interfacial Galvani potential difference ($\Delta^{\mathrm{w}}_{\mathrm{o}}\phi$ / V) using a four-electrode or two-electrode electrochemical cell for macroITIES or micro-/nano-ITIES experiments, respectively. This process is described by the Nernst-Donnan equation:[6,7]

$$\Delta^{\mathrm{w}}_{\mathrm{o}}\phi = \Delta^{\mathrm{w}}_{\mathrm{o}}\phi_i^{\ominus\prime} + \frac{RT}{z_i F}\ln\left(\frac{c^{\mathrm{o}}_{i,x=0}}{c^{\mathrm{w}}_{i,x=0}}\right) \qquad (1)$$

where $\Delta^{\mathrm{w}}_{\mathrm{o}}\phi_i^{\ominus\prime}$ is the formal transfer potential of the ion, and z_i is the charge on that ion. It is important to state that the Nernst-Donnan equation depends on the interfacial concentrations of the ion at both sides of the interface, *i.e*, when *x*=0. The physical model assumes that a two-dimensional interface exists. Therefore, the thickness of the interface is equal to zero and *x*=0 is the position of the plane that separates both liquid phases. Thus, the soft ITIES plays the role typically occupied by a classical solid-state working electrode (*e.g.*, gold, glassy carbon, or indium tin oxide (ITO)) as the transducer in the electrochemical cell.

Examples of redox-inactive ions quantitatively detected by their reversible ion transfer across the ITIES include drugs, such as cocaine,[8] propranolol,[9–11] metoprolol,[12] daunorubicin[13] topotecan,[14] antimicrobial drug ions (quinolones and sulfonamides)[15] and fluoroquinolone antibiotics,[16] neurotransmitters and neuromodulators such as dopamine,[17–21] acetylcholine,[22–26] tryptamine,[26] serotonin[26] and gamma-aminobutyric acid,[27] pathogenic bacterial quorum sensing molecules such as 4-hydroxy-2-heptylquinoline (HHQ) and 2-heptyl-3,4-dihydroxyquinoline (pseudomonas quinolone signal, PQS),[28] and heavy metal ion

environmental toxins such as Pb(II),[29,30] Cd(II)[18,29–35] and Cr(VI).[36,37] Comprehensive overviews of recent developments in this fast-evolving field can be found in reviews by Arrigan,[38–41] Dassie,[42] Herzog,[43] Lee,[44] Shen[45] and their co-workers.

The primary electrochemical techniques used to date to generate the electroanalytical signal at the ITIES in the presence of redox-inactive ions are amperometry[46–52] and voltammetry (cyclic voltammetry (CV)[8,16,28,53–55] and differential pulse voltammetry (DPV),[21,40,56,57] respectively). Successful application of these methods to achieve precise quantitative analysis at the macroITIES can be hampered by the presence of interfering capacitive currents, background currents due to residual ion transfer of the aqueous electrolyte across the full polarisable potential window (PPW), and the inherently high resistance of a liquid|liquid (L|L) electrochemical cell due to the presence of an organic phase.[58,59] The most successful approach to date to overcome these limitations, achieving in some cases sub-nanomolar quantification of organic or inorganic ions, is the combination of interfacial miniaturisation to the micro- or nano-scale and differential pulse stripping voltammetry (DPSV).[39,43,60–66]

Herein, to improve the relationship between the electroanalytical signal at the macroITIES and concentration of redox-inactive ions present, a new approach has been developed using alternating current (AC) voltammetry, also known as potentiodynamic electrochemical impedance spectroscopy (PEIS) at a single frequency. While AC voltammetry has been used extensively to support mechanistic analysis of ion adsorption and transfer at the ITIES,[58,59,67,68] its application for quantitative analysis has been overlooked.

Conventional AC voltammetry uses AC current as an analytical signal. However, in this article, we describe an approach to define a novel analytical signal by extracting from the total impedance the component that depends only on the Warburg element. The latter is a function of the interfacial ion concentration and diffusion coefficient, as well as the temperature, and serves as the "analytical signal" herein. A key advantage of electrochemical impedance spectroscopy (EIS) over amperometry, CV, DPV or square wave voltammetry (SWV) is that it avoids the use of positive feedback *iR* compensation, which reduces the stability of the potentiostat and may lead to severe ringing or oscillation, especially when macroITIES (with cm^2 or mm^2 interfacial areas) are used. This latter effect may be particularly detrimental when using a L|L electrochemical cell due to the high resistance of the organic phase electrolyte. Thus, applying AC voltammetry as an electroanalytical technique has major

potential to enhance the robustness of electrochemical sensors designed using soft macroITIES as the transducer.

Experimental Section

Materials. All chemicals were used as received without further purification. All aqueous solutions were prepared with ultrapure water (Millipore Milli-Q, specific resistivity 18.2 MΩ·cm). Bis(triphenylphosphoranylidene) ammonium chloride (BACl, 97%) and lithium tetrakis(pentafluorophenyl)borate diethyletherate ([Li(OEt_2)]TB) were obtained from Sigma-Aldrich and Boulder Scientific Company, respectively. Bis(triphenylphosphoranylidene)ammonium tetrakis(pentafluorophenyl)borate (BATB) was prepared as reported previously.[59] Tetramethylammonium chloride (TMACl, 98%), tetraethylammonium chloride (TEACl, 98%) and tetrapropylammonium chloride (TPACl, 98%) were obtained from Sigma-Aldrich. The organic solvents α,α,α-trifluorotoluene (TFT, 99%) and 1,2-dichloroethane (DCE, 99.8%) were obtained from Acros Organics.

Cyclic voltammetry and electrochemical impedance spectroscopy (EIS) at the ITIES. Electrochemical experiments were carried out at an aqueous|TFT or aqueous|DCE interface using a four-electrode configuration (the geometric area of the L|L interface was 1.60 cm^2), see Figure S1. To supply the current flow, platinum counter electrodes were positioned in both the aqueous and organic phases. The potential drop at the L|L interface was measured by means of silver/silver chloride (Ag/AgCl) electrodes, which were connected to the aqueous and organic phases, respectively, through Luggin capillaries. Calibration of the voltammetry to the Galvani potential scale was achieved by assuming the formal ion transfer potential ($\Delta_o^w \phi_i^{\ominus\prime,w\to o}$) of TMA^+ to be 0.311 V at the aqueous|TFT interface[69] and 0.160 V at the aqueous|DCE interface.[70] The general configuration of the cell is outlined in Scheme 1. From this point on, we specify only the composition of the aqueous and organic phases as all other elements of the four-electrode electrochemical cell were kept constant.

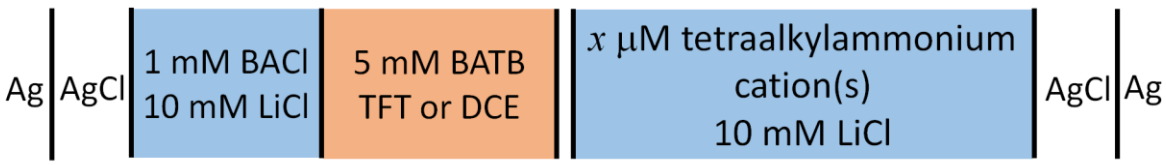

Scheme 1. The general configuration of the four-electrode electrochemical cell used for cyclic voltammetry, electrochemical impedance spectroscopy (EIS) and AC voltammetry measurements. The aqueous electrolyte composition was varied between studies. The organic electrolyte solution was either α,α,α-trifluorotoluene (TFT) or 1,2-dichloroethane (DCE) containing 5 mM bis(triphenylphosphoranylidene)ammonium tetrakis(pentafluorophenyl)-borate (BATB) as the supporting electrolyte.

Electrochemical impedance spectroscopy (EIS) spectra were measured using an Autolab PGSTAT204 potentiostat, equipped with a FRA32M frequency response analyser, connected to a four-electrode electrochemical cell. The AC amplitude was 10 mV and the frequency range was between 0.1 and 300 Hz. The upper limit of the frequency range was restricted to 300 Hz because at higher frequencies the electrolytes do not behave as an ideal resistors.[59] The potentiostat was connected to an uninterruptible power supply (APC by Schneider Electric) to ensure voltage stability and remove an inductive artefact at high frequencies. The differential capacitances and imaginary parts of the Warburg element at different applied voltages were measured using AC voltammetry (also known as PEIS at a single frequency) at frequencies between 1 and 100 Hz and assuming that the cell behaves as a Randles circuit. The step potential for the latter experiments was 10 mV. The working temperature was 20 ± 2 °C.

Results and discussion

The limitations of voltammetry at the ITIES for electroanalysis. A cyclic voltammogram of the reversible ion transfer of the redox-inactive tetraalkylammonium cations TPA^+ and TMA^+ at the macroITIES is shown in Figure 1a (solid black line). Comparison with the blank cyclic voltammogram (solid red line) demonstrates the challenge associated with deconvoluting the Faradic currents, that constitute the analytical signal, from the interfering capacitive and background ionic currents.[59] The capacitive currents change significantly with the applied $\Delta_o^w\phi$ (Figure 1a) and the background ionic current changes depending on the chosen width of the potential range (Figure 1b). Thus, in the absence of a clear baseline, an accurate quantitative analysis of the tetraalkylammonium cation concentration with high accuracy through measurement of the peak heights is not feasible.

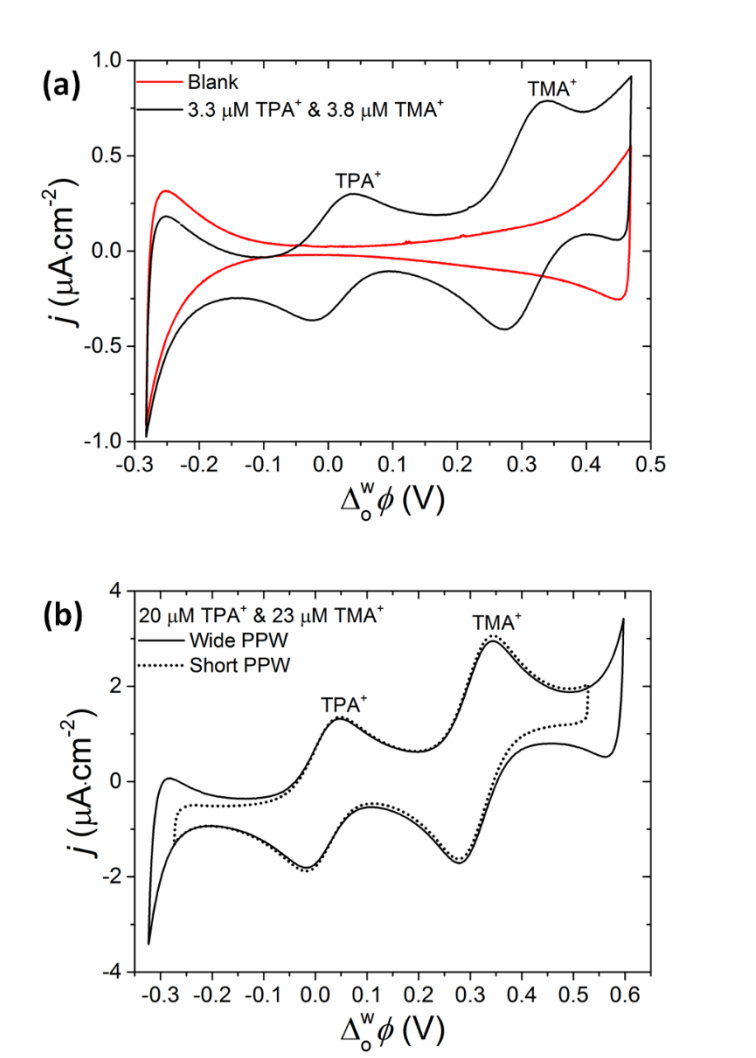

Figure 1. (a) Cyclic voltammograms obtained in the absence (solid red line) and presence of 3.3 μM TPA^+ and 3.8 μM TMA^+ (solid black line) in the aqueous phase. **(b)** The effect of the width of the potential range on the background currents of the voltammograms. The concentrations of the tetraalkylammonium cations were 20 μM TPA^+ and 23 μM TMA^+, respectively. The configuration of the four-electrode electrochemical cell was as described in Scheme 1 with TFT as the organic solvent. The scan rate used was 25 $mV \cdot s^{-1}$.

Theoretical background underpinning the use of AC voltammetry at the macroITIES for electroanalysis. Impedance data provide a much more nuanced and complete description of an electrochemical system in comparison to standard voltammetry experiments, the underlying reasons for which are summarised eloquently in the opening introduction to Chapter 10 of "Electrochemical Methods, Fundamentals and Applications" by Bard and Faulkner.[71] Thus, to thoroughly understand the four-electrode electrochemical cell described

in Scheme 1, EIS spectra were taken at the $\Delta_{\mathrm{o}}^{\mathrm{w}}\phi_i^{\ominus',\mathrm{w}\to\mathrm{o}}$ of TMA^+ (0.311 V) and TPA^+ (0.013 V) at the aqueous|TFT interface (see Figure S2 and Table S1). These EIS spectra were simulated using the equivalent circuit shown in Scheme 2. The total impedance (Z) of this circuit is:

$$Z = R_{\mathrm{s}} + \frac{Z_W Z_C}{(Z_W + Z_C)} \qquad (2)$$

$$Z = R_s + \frac{\sigma\omega^{-1/2}[1-j(1+2C_{\mathrm{d}}\omega^{1/2}\sigma)]}{(1+2C_{\mathrm{d}}\omega^{1/2}\sigma+2\omega(C_{\mathrm{d}}\sigma)^2)} \qquad (3)$$

where the Warburg impedance $Z_{\mathrm{W}} = \sigma(1-j)\omega^{-1/2}$ and the capacitance $Z_C = 1/j\omega C_d$. The term $j = \sqrt{(-1)}$, ω is the angular frequency, C_{d} is the differential capacitance of the double layer and σ is the Warburg coefficient. In turn, the real (Z_{Re}) and imaginary (Z_{Im}) impedances are

$$Z_{\mathrm{Re}} = R_s + \frac{\sigma}{(\omega^{1/2}(1+2C_{\mathrm{d}}\omega^{1/2}\sigma+2\omega(C_{\mathrm{d}}\sigma)^2))} \qquad (4)$$

$$Z_{\mathrm{Im}} = -\sigma\left(\frac{1+2C_{\mathrm{d}}\omega^{1/2}\sigma}{(\omega^{1/2}(1+2C_{\mathrm{d}}\omega^{1/2}\sigma+2\omega(C_{\mathrm{d}}\sigma)^2))}\right) \qquad (5)$$

Equations (4) and (5) show that Z_{Re} depends on the electrolyte resistance, R_s, whereas Z_{Im} is independent of this value. Therefore, as Z_{Im} does not depend on the electrolyte resistance, it is far more suited to electroanalytical applications at the ITIES than Z_{Re}. Thus, taking into account the equality $\sigma = 1/Y_0\sqrt{2}$, where Y_0 is the Warburg admittance factor, the elements Z_C and Z_{W} in the equivalent circuit are accounted for in the simulation by the parameters C_{d} and Y_0, respectively. The values of the different parameters (R_s, C_{d} and Y_0) obtained after fitting are shown in Table S1, with low errors in each case as determined from the non-linear fitting process between the experimental data and the equivalent circuit shown in Scheme 2 using the NOVA software of the Autolab PGSTAT204 potentiostat.

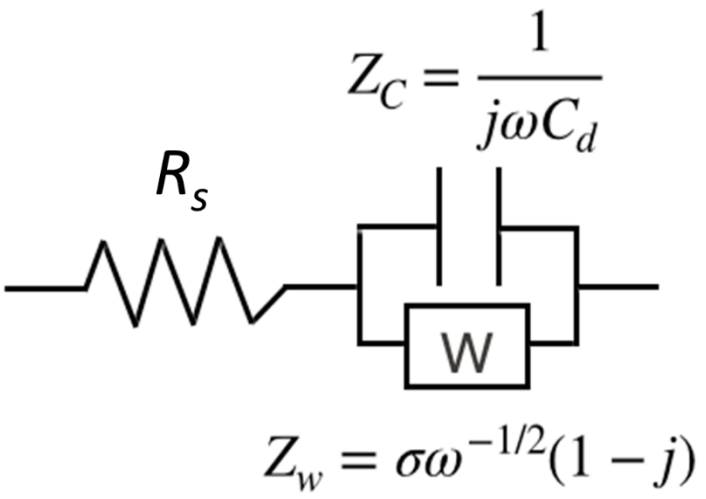

Scheme 2. The equivalent circuit used to simulate the electrochemical impedance spectra obtained at a polarised aqueous|TFT or aqueous|DCE interface using a four-electrode configuration as described in Scheme 1. R_s is the solution resistance, Z_W is the Warburg impedance, and Z_C is the interfacial capacitance.

In controlled-potential electrochemical methods, the uncompensated solution resistance, R_s, causes two problems: a potential control error due to *iR* drop and a slow cell response due to a finite cell time constant.[72] In the case of a macroITIES, a significant source of error is the compensated or uncompensated ohmic potential drop due mainly to the organic electrolyte solution resistance.[59] Table S1 shows that the total solution resistance, R_s, of the L|L electrochemical cell used herein is ca. 1 kΩ, in agreement with previous studies.[59] However, as the value of the charge transfer resistance, R_{ct}, is more than two orders of magnitude lower,[7] it is too small to calculate from the EIS spectra and it was not taken into account in the model to simulate the EIS spectra (see Scheme 2 and Table S1).Thus, although in previous studies the Faradaic impedance (Z_F) at the ITIES was written as the sum of R_{ct} and Z_W,[73,74] herein it is represented by solely Z_W.

The deconvolution of Z_W, which depends on the interfacial analyte concentration at the ITIES, can be carried out as follows. First, σ, the Warburg coefficient, is a parameter defined as:

$$\sigma = \frac{RT}{z_i^2 F^2 A\sqrt{2}}\left[\frac{1}{\sqrt{D_i^o}c_{i,x=0}^o} + \frac{1}{\sqrt{D_i^w}c_{i,x=0}^w}\right] \qquad (6)$$

where A is the area of the L|L interface, D_i^{o} and D_i^{w} are the diffusion coefficients of i in the aqueous or organic phase, respectively, z_i is the relative charge of the transferred ion and R, T, and F have their usual meanings. At $\Delta_{\mathrm{o}}^{\mathrm{w}}\phi_i^{\ominus',\mathrm{w}\to\mathrm{o}}$, $c_{i,x=0}^{\mathrm{o}} = c_{i,x=0}^{\mathrm{w}}$ and the interfacial ion concentration is assumed to be $c_{i,x=0}^{\mathrm{w}} = \left(c_{i,\mathrm{bulk}}^{\mathrm{w}}/2\right)$. In this sense, Equation (6) can be simplified to:

$$\sigma \approx \frac{2RT}{c_{i,\mathrm{bulk}}^{\mathrm{o}} z_i^2 F^2 A\sqrt{2}}\left[\frac{1}{\sqrt{D_i^{\mathrm{o}}}} + \frac{1}{\sqrt{D_i^{\mathrm{w}}}}\right] \qquad (7)$$

Equation (7) clearly shows that the inverse of σ is proportional to the bulk concentration at $\Delta_{\mathrm{o}}^{\mathrm{w}}\phi_i^{\ominus',\mathrm{w}\to\mathrm{o}}$. Taking only the imaginary part of the impedance (Z_{Im}), the term gamma (γ) is calculated as follows:

$$\gamma = -\frac{1}{\omega Z_{\mathrm{Im}}} = \frac{1}{\omega^{1/2}\sigma} + \frac{2\omega(C_d\sigma)^2}{\sigma\omega^{1/2}\left(1+2C_d\omega^{1/2}\sigma\right)} \qquad (8)$$

If $2C\omega^{1/2}\sigma \gg 1$ and, as noted earlier, $\sigma = 1/Y_0\sqrt{2}$, the γ term is simplified to:

$$\gamma = \frac{Y_0\sqrt{2}}{\omega^{1/2}} + C_{\mathrm{d}} \qquad (9)$$

Equation (9) indicates that at a certain frequency ω, determined experimentally for any four-electrode cell configuration studied, AC voltammetry can be used in the presence of an ionic analyte to calculate γ as a function of $\Delta_{\mathrm{o}}^{\mathrm{w}}\phi$. On the other hand, the C_{d} *vs.* $\Delta_{\mathrm{o}}^{\mathrm{w}}\phi$ curve can also be calculated using the same technique in the absence of any analyte (the "blank" scan). Subtracting C_{d} from γ (at each $\Delta_{\mathrm{o}}^{\mathrm{w}}\phi$ value) yields the term $\frac{Y_0\sqrt{2}}{\omega^{1/2}}$ that is effectively the analytical signal. For clarity, the treatment of raw AC voltammetry dataset in this manner is outlined in the Supporting Information (see Tables S2 & S3).

A key point when using AC voltammetry for electroanalytical applications with L|L electrochemical cells is to recognise that not all L|L interfaces behave the same. The theoretical model (*i.e.*, the equivalent circuit described in Scheme 2) used herein is optimal for use with similarly behaving aqueous|TFT and aqueous|DCE interfaces. However, if other L|L interfaces are formed, in particular for more complicated systems with realistic analytical matrices such as river water|organic, serum|organic or urine|organic interfaces, a new equivalent circuit must be determined for each that accurately simulates the EIS spectra. Such an equivalent circuit in a realistic sample may need to introduce elements that consider the accumulation or adsorption of different species, such as proteins or surfactants, at the L|L interface or currents arising from

electron transfer as well as ion transfer processes. Furthermore, many species may transfer at the same $\Delta_o^w\phi$. Then, using the optimal theory for the chosen L|L interface, deconvolution of the analytical signal can be done using AC voltammetry as described in this article.

Proof-of-concept experiments using AC voltammetry at the ITIES to quantitatively detect redox-inactive ions. The γ vs. $\Delta_o^w\phi$ curve obtained by AC voltammetry at a frequency of 1 Hz in the presence of two tetraalkylammonium cations (TPA^+ and TMA^+) is shown in Figure 2a (solid black line). The Faradaic signals are clearly superimposed upon the purely capacitive curve (solid red line) obtained with an identical cell configuration in the absence of the tetraalkylammonium cations. The intensity of the Faradaic response in the γ vs. $\Delta_o^w\phi$ curve depends on the chosen frequency for AC voltammetry, with the highest intensity and a stable baseline observed with 1 Hz (Figure 2b). The intensity dropped significantly upon choosing progressively higher frequencies of 5 and 99 Hz, respectively. Indeed, the intensity of the Faradaic response is so low at 99 Hz, that this frequency can be chosen to measure C_d with good accuracy even in the presence of the tetraalkylammonium cations. Ion transfer is a diffusion-limited process. Thus, a low frequency of 1 Hz in AC voltammetry will provide a sufficiently long time-frame of voltage excitation to enhance any reversible Faradaic ion transfer signal (and *vice versa* for high frequencies). Nevertheless, during each 10 mV step-potential, the effect of the excitation frequency will depend on the ion's nature (*e.g.*, charge, solvation or diffusion coefficient).

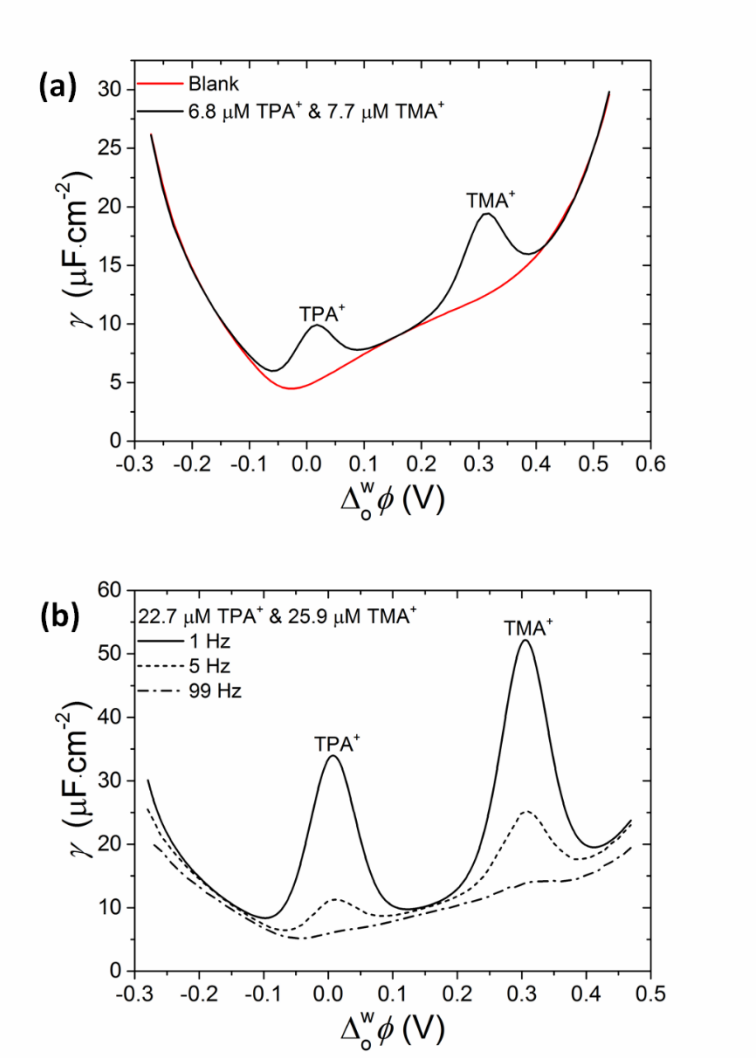

Figure 2. (a) γ *vs.* $\Delta_o^w\phi$ curves obtained in the absence (solid red line line) and presence (solid black line) of 6.8 μM TPA^+ and 7.7 μM TMA^+ in the aqueous phase. The frequency used to obtain the AC voltammograms was 1 Hz. **(b)** The effect of the applied frequency on the AC voltammetry. All γ *vs.* $\Delta_o^w\phi$ curves were obtained in the presence of 22.7 μM TPA^+ and 25.9 μM TMA^+, respectively. The configuration of the four-electrode electrochemical cell was as described in Scheme 1 with TFT as the organic solvent. The minimal effect of the applied frequency on the AC voltammetry of blank electrochemical cells, in the absence of TPA^+ and TMA^+, is shown in Figure S3.

Control "blank" experiments were carried out, with C_d *vs.* $\Delta_o^w\phi$ curves obtained for the electrochemical cell at different frequencies, from 1 to 99 Hz, in the presence of only supporting electrolytes in each liquid phase (Figure S3). No artefacts were associated with these blanks, with all curves showing minimal deviations of the interfacial capacitances

between –0.2 V and 0.3 V. At the edges of the potential range the deviation is higher due to the contribution of background ionic currents, which are more important at low frequencies.

Figure 2a also shows that the background ionic currents[59] observed in Figure 1a are not detected by AC techniques, *i.e.* the baseline at the edges of the potential range come from only capacitive currents and are very stable (Figure S3). A further key point is that AC voltammetry can detect only reversible electrochemical reactions, and thus Figure 2a only shows reversible processes such as the charge and discharge of the interfacial capacitor and the ionic transfer of TMA^+ and TPA^+. Irreversible processes do not give an AC signal and quasi-reversible processes lead to a small AC signal.

A quantitative analysis was performed by measuring analytical signal $\frac{Y_0\sqrt{2}}{\omega^{1/2}}$ *vs.* $\Delta_o^w\phi$ curves in the presence of increasing concentrations of TPA^+ and TMA^+, respectively (Figure 3a). The baseline and peak positions were found to be very stable and the peak shapes were highly symmetrical. Such characteristics are ideal for analytical applications and, indeed, plots of the tetraalkylammonium cation concentrations *vs.* the analytical signal $\frac{Y_0\sqrt{2}}{\omega^{1/2}}$ yielded good linearity over the concentration range of $2 - 30$ μM studied. (Figure 3b).

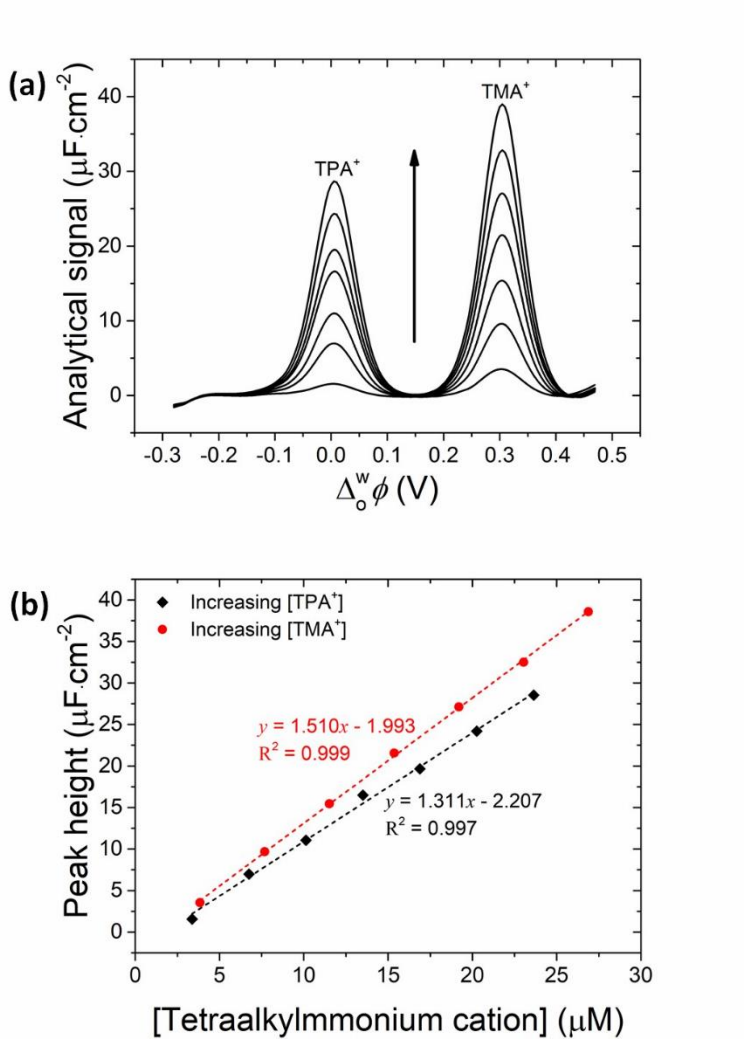

Figure 3. (a) Analytical signal $\frac{Y_0\sqrt{2}}{\omega^{1/2}}$ *vs.* $\Delta_o^w\phi$ curves in the presence of increasing concentrations of TPA^+ and TMA^+ in the aqueous phase. **(b)** Linear fitting between peak height and the concentration of TMA^+ (solid red circles) or TPA^+ (solid black diamonds). Statistical data of linear trend estimations are provided in Table S4. The configuration of the four-electrode electrochemical cell was as described in Scheme 1 with TFT as the organic solvent. The frequency used to obtain the AC voltammograms was 1 Hz.

The limit of detection (LOD) and limit of quantification of TMA^+ are 0.5 μM and 1.6 μM, respectively. For TPA^+ those values are 1.3 μM and 4.4 μM, respectively. The LOD and the limit of quantification were taken as 3 and 10 times the standard deviation of the peak heights, respectively. To our knowledge, these are the best LODs of any electroanalytical technique using macroscopic (centimeter sized) L|L interfaces reported to date for the detection of tetraalkylammonium cations. Cyclic voltammetry can typically only achieve LODs >10 μM

for tetraalkylammonium cations,[75] while the previous state-of-the-art was an LOD of 5.9 μM for the detection of TMA^+ using square wave voltammetry (SWV) at an aqueous|nitrobenzene interface,[76] still ten times higher than demonstrated herein with AC voltammetry. Other electroanalytical techniques, such as DPSV combined with gellifying the organic phase (to implement a pre-concentration step) and interfacial miniaturisation to the micro- or nano-scale can achieve superior LODs, in the sub-nanomolar range, based on ion transfer across the ITIES.[60–65] However, both DPSV[66] and in particular SWV[76] suffer from less stable baseline signals and asymmetry of the peak shapes, complicating the accurate calculation of $\Delta_o^w \phi_i^{\ominus',w\to o}$, the peak heights or areas in comparison to that achieved by AC voltammetry.

The diffusion coefficient of an ion in TFT can be calculated if (i) the diffusion coefficient in water is known and (ii) using Equations (7) and (8), the slopes of the trendlines in Figure 3b (m) are determined. The working equation is:

$$\frac{2m^2R^2T^2\omega}{F^4} = \frac{D_i^o D_i^w}{\left(\sqrt{D_i^o}+\sqrt{D_i^w}\right)^2} \qquad (10)$$

For example, taking into account that the slope (m) for TMA^+ in SI units is 15.1 $C^2 \cdot m \cdot mol^{-1} \cdot J^{-1}$ and the diffusion coefficient of this ion in water at 293 K is 9.5 x 10^{-10} $m^2 \cdot s^{-1}$,[77] the calculated diffusion coefficient of TMA^+ in TFT is 6.6 x 10^{-10} $m^2 \cdot s^{-1}$ at 293K. Using the reported diffusion coefficient for TPA^+ in water at 25 °C of 8.2 x 10^{-10} m^2 s^{-1},[78] and slope of 13.1 $C^2 \cdot m \cdot mol^{-1} \cdot J^{-1}$ from Figure 3b, the calculated diffusion coefficient of TPA^+ at 293 K in TFT is 4.5 x 10^{-10} m^2 s^{-1}. As expected from the respective mobilities of the ions in water, the diffusion coefficient of TMA^+ is also higher than that for TPA^+ in TFT. Furthermore, both diffusion coefficient values in TFT are lower than those in water since the TFT viscosity is higher than water viscosity at 293 K, which are 0.5740 N s m^{-2} and 0,001 N s m^{-2} respectively.[79] To our knowledge, the diffusion coefficients of tetraalkylammonium ions in TFT have not been reported previously. However, comparisons of the above values to those reported in nitrobenzene (2.7 x 10^{-10} $m^2 \cdot s^{-1}$ for TMA^+ and 4.5 x 10^{-10} $m^2 \cdot s^{-1}$ for TPA^+)[80] are quite reasonable. In this regard, the consistency of the above calculations shows that the proposed methodology to quantify the tetraalkylammonium ions is very precise and also very useful to measure physical constants such as the diffusion coefficients of ions in both liquid phases.

Exploring the limitations of AC voltammetry at the ITIES for electroanalysis. Despite the stable baseline observed for the analytical signal $\frac{Y_0\sqrt{2}}{\omega^{1/2}}$ *vs.* $\Delta_o^w \phi$ curves in the

presence of increasing concentrations of TPA^+ and TMA^+ (Figure 3a), the linear fitting of the peak heights *vs.* concentration of tetraalkylammonium cations reveals a negative intercept for both TPA^+ and TMA^+ (Figure 3b and Table S4). This may be attributed to modest changes in the baseline in the presence of the tetraalkylammonium cations at $\Delta_o^w\phi$ values corresponding to their $\Delta_o^w\phi_i^{\ominus\prime,w\to0}$ values. However, the baseline remains fully stable at applied $\Delta_o^w\phi$ values away from the Faradaic signals, *e.g.*, in the range $-0.30\ \text{V} < \Delta_o^w\phi < -0.15\ \text{V}$ in Figure 3a.

In order to study the stability of the baseline during ion transfer, EIS spectra were taken at $\Delta_o^w\phi_i^{\ominus\prime,w\to o}$ values of 0.311 V and 0.013 V for TMA^+ and TPA^+, respectively, with increasing tetraalkylammonium cation concentrations in the aqueous phase. The double-layer capacitance (C_d) of the polarised L|L interface was calculated by fitting the EIS spectra at each cation concentration to the equivalent circuit shown in Scheme 2. In both cases, C_d increases with the tetraalkylammonium cation concentrations (Figure 4). The values of the different parameters (R_s, C_d and Y_0) obtained after fitting for each concentration of TPA^+ and TMA^+ in the aqueous phase are shown in Table S1, with low errors in each case. Furthermore, as a representative example, the excellent match between the experimental impedance spectra and modelled equivalent circuit is shown in Figure S2 with 22.7 μM TPA^+ in the aqueous phase.

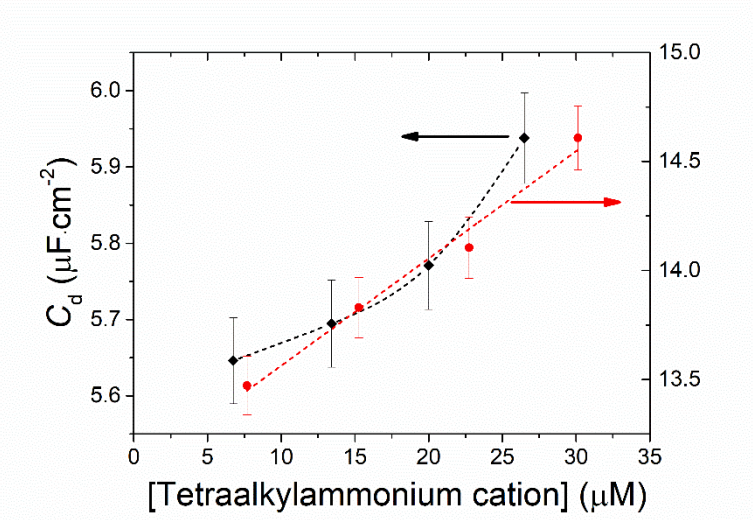

Figure 4. Double-layer capacitance (C_d) of the L|L interface at the formal ion transfer potentials ($\Delta_o^w\phi_i^{\ominus\prime,w\to0}$) of TMA^+ (0.311 V; solid red circles) and TPA^+ (0.013 V; solid black diamonds), respectively, *vs*. their concentration in the aqueous phase. The configuration of the four-electrode electrochemical cell was as described in Scheme 1 with TFT as the organic

solvent. Using the equivalent circuit described in Scheme 2, the maximum error obtained in the estimation of the capacitance was 1%.

The Gouy-Chapman-Stern model predicts that C_d increases with the ionic strength.[81] However, the concentrations of the tetraalkylammonium salts are more than two orders of magnitude lower than the supporting electrolyte. This suggests that the ionic strength is not changing to a significant degree, and the observed increases in C_d may instead be due to the transient adsorption of the tetraalkylammonium cations at the interface during the course of the heterogeneous ion transfer. Such transient adsorption events have been reported previously by Samec and co-workers for tetraalkylammonium cations,[82] as well as for other ions such as the Rose Bengal dianion,[83] and Erythrosine B dianions and Eosin Y dianions.[84]

The aqueous|TFT interface provides one of the widest accessible PPWs for polarised ITIES studies.[85] On the other hand, the PPW of a polarised aqueous|DCE interface is considerably shorter (Figure 5a). A cyclic voltammogram at the aqueous|DCE interface in the presence of 2.56 μM TMA^+, 2.25 μM TEA^+ and 2.25 μM TPA^+ in the aqueous phase is shown in Figure 5b. As described earlier, cyclic voltammetry does not allow a clear deconvolution of the Faradic currents related to each tetraalkylammonium cation. Also, as evident from the cyclic voltammograms, TPA^+ undergoes ion transfer far closer to the negative edge of the PPW at the aqueous|DCE interface (Figure 5b) than is the case at the aqueous|TFT interface (Figure 1a).

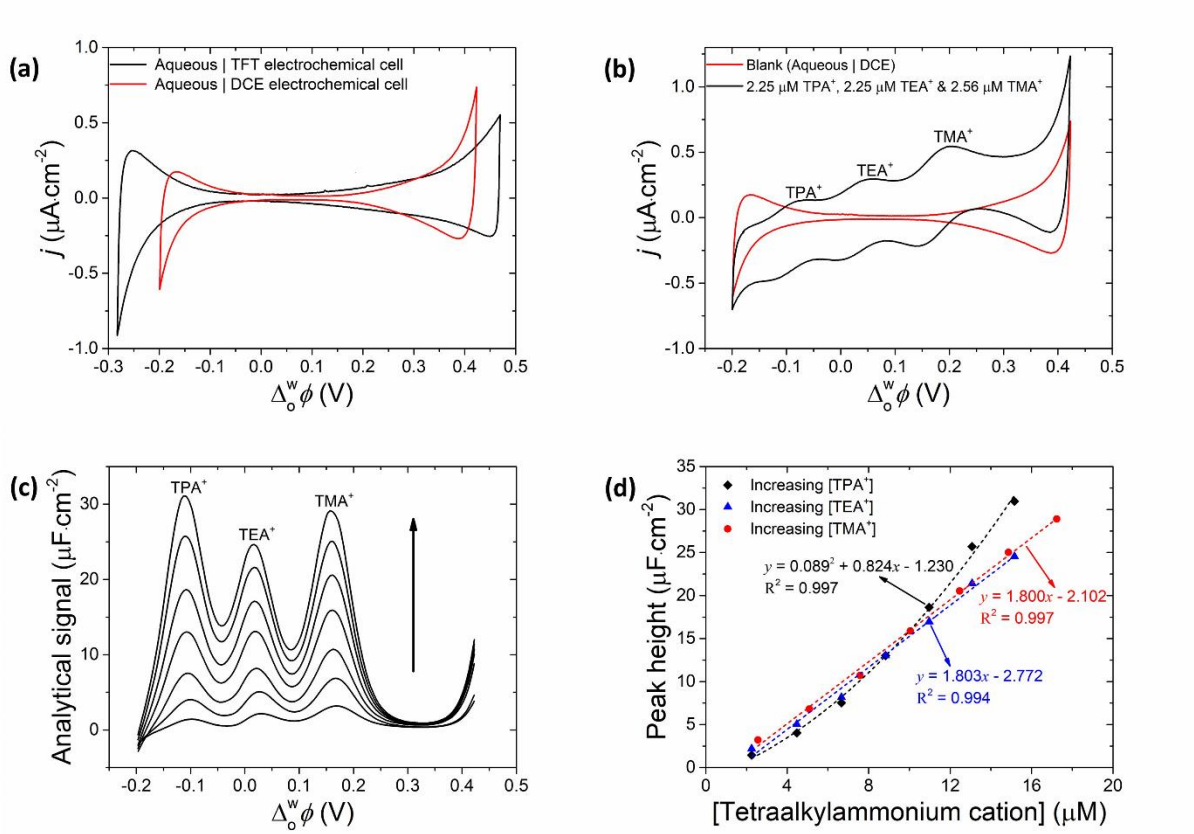

Figure 5. (a) Comparing the width of the PPW obtained by cyclic voltammetry using the configuration of the four-electrode electrochemical cell described in Scheme 1 with either TFT (black solid line) or DCE (red solid line) as the organic solvent. The scan rate used was 25 mV·s^{-1} **(b)** Cyclic voltammograms obtained in the absence (solid red line) and presence of 2.25 μM TPA^+, 2.25 μM TEA^+ and 2.56 μM TMA^+ (solid black line) in the aqueous phase. The scan rate used was 25 mV·s^{-1}. **(c)** Analytical signal $\frac{Y_0\sqrt{2}}{\omega^{1/2}}$ *vs.* $\Delta^{w}_{o}\phi$ curves in the presence of increasing concentrations of TPA^+, TEA^+ and TMA^+ in the aqueous phase. The frequency used to obtain the AC voltammograms was 1 Hz. **(d)** Linear fitting between peak height and the concentration of TMA^+ (solid red circles), TEA^+ (solid blue triangles) or TPA^+ (solid black diamonds). Statistical data of linear trend estimations are provided in Table S5. In panels (b), (c) and (d), the configuration of the four-electrode electrochemical cell was as described in Scheme 1 with DCE as the organic solvent.

A quantitative analysis was performed at the aqueous|DCE interface by measuring analytical signal $\frac{Y_0\sqrt{2}}{\omega^{1/2}}$ *vs.* $\Delta^{w}_{o}\phi$ curves in the presence of increasing concentrations of TPA^+, TEA^+ and TMA^+, respectively (Figure 5c). Plots of the tetraalkylammonium cation

concentrations *vs.* the analytical signal $\frac{Y_0\sqrt{2}}{\omega^{1/2}}$ yielded good linearity over the concentration range of 2 − 18 μM studied for TMA^+ and TEA^+, but not TPA^+ (Figure 5d and Table S5). Interestingly, the quality of the linear fitting decreases in the order $TMA^+ > TEA^+ > TPA^+$. The shorter PPW at the aqueous|DCE interface will inevitably lead to some analyte ions transferring nearer the positive and negative potential extremes, where interfering processes such as ion transfer of the aqueous background electrolyte may hamper the analytical performance of AC voltammetry. In this regard, Figures 5c and d can be interpreted as showing that the baseline for the TPA^+ Faradaic response is affected by current related to background chloride (Cl^-) transfer. Furthermore, the concentration of the interfering Cl^- species will increase as the concentration of the tetraalkylammonium chloride salts increase. In addition, the adsorption of increasing concentrations of tetraalkylammonium cations can reduce the interfacial surface tension at all $\Delta_o^w\phi$ values, but in particular at potentials approaching their $\Delta_o^w\phi_i^{\ominus',w\to o}$. A reduced interfacial surface tension will enhance the ease of ion transfer of both the tetraalkylammonium cations and background electrolyte species leading to deviations in the linearity of the analytical response over the concentration range. In particular, the adsorption of the more hydrophobic TPA^+ at the water|*n*-hexane interface has been well characterised.[86]

EIectroanalysis with AC voltammetry at the ITIES when "blank" measurements with zero concentrations of analyte are not possible. In real sample matrices, a blank may not always be possible due to the presence of trace concentrations of the analyte in the media, *e.g.*, as is often the case with metallic ions in drinking water.[87] A successful approach pioneered by Bonfil *et al.*[88–91] to circumvent the need for a "blank" to enhance the resolution of the Faradaic responses for a mixture of analytes and/or lower the limits of detection (LOD) was the development of subtractive anodic stripping voltammetry (SASV This technique involves carrying out an initial voltammetric scan using a preconcentration time, *t*, for periods in the order of minutes, followed by a second scan under the same experimental conditions but using no preconcentration time ($t = 0$). The latter effectively acts as the "blank" scan and is subtracted from the first scan. Herein, Figure 2b clearly demonstrates that Faradaic *vs.* capacitive processes at the ITIES can be easily differentiated by running a series of AC voltammograms using progressively higher applied frequencies. Thus, in a similar vein to SASV, one AC voltammogram can be obtained at an initial frequency that maximises the Faradaic response (1 Hz in Figure 2a) and a second at another frequency that maximises the capacitive response (99 Hz in Figure 2a). The latter AC voltammogram now effectively acts as the "blank" to generate

the analytical signal $\frac{Y_0\sqrt{2}}{\omega^{1/2}}$ in situations when a "blank" with zero concentration of analyte, *i.e.*, C_d in Equation (9), is not available. The excellent correlation between the analytical signal $\frac{Y_0\sqrt{2}}{\omega^{1/2}}$ *vs.* $\Delta_\mathrm{o}^\mathrm{w}\phi$ curves generated by subtracting the AC voltammograms obtained either (i) in the absence of ions at 1 Hz (solid black line), or (ii) in the presence of ions at 99 Hz (dashed black line), from the AC voltammogram obtained in the presence of the ions at 1 Hz is shown in Figure 6.

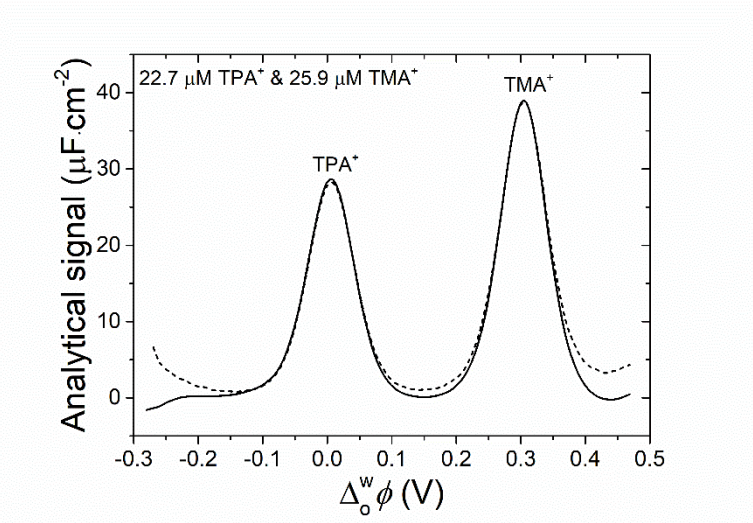

Figure 6. Analytical signal $\frac{Y_0\sqrt{2}}{\omega^{1/2}}$ *vs.* $\Delta_\mathrm{o}^\mathrm{w}\phi$ curves in the presence of 22.7 μM TPA^+ and 25.9 μM TMA^+ in the aqueous phase. To generate the analytical signal $\frac{Y_0\sqrt{2}}{\omega^{1/2}}$ *vs.* $\Delta_\mathrm{o}^\mathrm{w}\phi$ curves, background subtraction was carried out with either a γ *vs.* $\Delta_\mathrm{o}^\mathrm{w}\phi$ curve obtained at 1 Hz in the absence of TPA^+ and TMA^+ in the aqueous phase (solid black line) or a γ *vs.* $\Delta_\mathrm{o}^\mathrm{w}\phi$ curve obtained at 99 Hz in the presence of TPA^+ and TMA^+ (dashed black line). The configuration of the four-electrode electrochemical cell was as described in Scheme 1 with TFT as the organic solvent.

Conclusions

Herein, we provide the theory underpinning, and experimental demonstration of, AC voltammetry as an outstanding electroanalytical technique to quantitively analyse redox-inactive ions at the macroITIES. To our knowledge, the LODs achieved are the best of any electroanalytical technique using such macroscopic (centimeter square sized) L|L interfaces reported to date for the detection of tetraalkylammonium cations (specifically TMA^+ and

TPA^+). The analytical signal is based on extracting the component that depends on the Warburg impedance (Z_w) from the total impedance (Z). The former is a function of the interfacial ion concentrations and diffusion coefficients. The quantitative detection of a series of model redox-inactive tetraalkylammonium cations, each of differing hydrophobicity and therefore formal ion transfer potential, $\Delta_o^w\phi_i^{\ominus\prime,w\to o}$, is demonstrated as a proof-of-concept. It was also demonstrated that this experimental approach is very useful to measure the diffusion coefficient in one phase if the diffusion coefficient in the other phase in known.

To investigate the stability of the baseline during ion transfer, the double-layer capacitance (C_d) of the polarised L|L interface was determined (by taking EIS spectra at potentials matching the $\Delta_o^w\phi_i^{\ominus\prime,w\to o}$ values for each cation) and found to increase in the presence of increasing cation concentrations. The latter was attributed to the transient adsorption of the tetraalkylammonium cations at the interface during the course of ion transfer. Transient adsorption may affect the linearity of the analytical response by reducing the interfacial surface tension, in particular at potentials approaching the $\Delta_o^w\phi_i^{\ominus\prime,w\to o}$, and thereby enhancing the ease of ion transfer of both the tetraalkylammonium cations and background electrolyte species. Nevertheless, the analytical signal generated using AC voltammetry has a more stable baseline and symmetrical shape than achieved with SWV[76] allowing highly accurate determination of $\Delta_o^w\phi_i^{\ominus\prime,w\to o}$, the peak heights or areas.

As is the case for all electroanalytical techniques at the ITIES, the linearity of the analytical response decreases for analyte ions that transfer near the edges of the polarisable potential window (PPW) due to current related to background electrolyte (Li^+ or Cl^-) transfer. In this regard, for a shorter PPW achieved by replacing the α,α,α-trifluorotoluene phase with 1,2-dichloroethane, the quality of the linear fitting decreases in the order TMA^+ > TEA^+ > TPA^+.

The modulation of the intensity of the Faradaic response due to ion transfer by changing the voltage excitation frequency during AC voltammetry opens major opportunities for the sensitive detection of ionic analyte under circumstances when a "blank" measurement in the absence of analyte is impossible. AC voltammetry will allow the deconvolution of interfering signals due to irreversible processes, which do not give AC signals, from those related to reversible ion transfer of a target analyte ion. Future work will focus on developing a deeper understanding of the effect of the AC excitation frequency on the Faradaic response for ions with substantially different nature's (*e.g.*, charge, solvation or diffusion coefficient). The

ultimate goal is to achieve the selective enhancement of the Faradaic response of the ionic target analyte, while "tuning out" the Faradaic signal of an interferent by manipulating the voltage excitation frequency.

Supporting Information

Schematic and image of the glassware of a four-electrode electrochemical cell, representative EIS spectrum and table of EIS parameters obtained at the formal ion transfer potential of the tetraalkylammonium cations, treatment of a raw AC voltammetry dataset to yield the analytical signal, blank AC voltammograms as a function of the applied frequency.

Author Contributions

The manuscript was written through contributions of both authors. Both authors have given approval to the final version of the manuscript.

Notes

The authors declare no competing financial interest.

Acknowledgements

M.D.S. acknowledges Science Foundation Ireland (SFI) under Grant no. 13/SIRG/2137 and the European Research Council through a Starting Grant (Agreement no. 716792). M.F.S.-H. acknowledges the "Universidad Nacional de Colombia" for allowing his sabbatical leave.

References

(1) Soda, Y.; Citterio, D.; Bakker, E. Equipment-Free Detection of K + on Microfluidic Paper-Based Analytical Devices Based on Exhaustive Replacement with Ionic Dye in Ion-Selective Capillary Sensors. *ACS Sensors* **2019**, *4* (3), 670–677. https://doi.org/10.1021/acssensors.8b01521.

(2) Suherman, A. L.; Rasche, B.; Godlewska, B.; Nicholas, P.; Herlihy, S.; Caiger, N.; Cowen, P. J.; Compton, R. G. Electrochemical Detection and Quantification of Lithium Ions in Authentic Human Saliva Using LiMn2O4-Modified Electrodes. *ACS Sensors* **2019**, *4* (9), 2497–2506. https://doi.org/10.1021/acssensors.9b01176.

(3) Li, S.; Zhang, C.; Wang, S.; Liu, Q.; Feng, H.; Ma, X.; Guo, J. Electrochemical Microfluidics Techniques for Heavy Metal Ion Detection. *Analyst* **2018**, *143* (18), 4230–4246. https://doi.org/10.1039/c8an01067f.

(4) Gumpu, M. B.; Sethuraman, S.; Krishnan, U. M.; Rayappan, J. B. B. A Review on Detection of Heavy Metal Ions in Water - An Electrochemical Approach. *Sensors Actuators, B Chem.* **2015**, *213*, 515–533. https://doi.org/10.1016/j.snb.2015.02.122.

(5) Bamsey, M.; Graham, T.; Thompson, C.; Berinstain, A.; Scott, A.; Dixon, M. Ion-Specific Nutrient Management in Closed Systems: The Necessity for Ion-Selective Sensors in Terrestrial and Space-Based Agriculture and Water Management Systems. *Sensors* **2012**, *12* (10), 13349–13392. https://doi.org/10.3390/s121013349.

(6) Peljo, P.; Girault, H. H. Liquid/Liquid Interfaces, Electrochemistry At. In *Encyclopedia of Analytical Chemistry*; John Wiley & Sons, Ltd: Chichester, UK, 2012. https://doi.org/10.1002/9780470027318.a5306.pub2.

(7) Samec, Z. Dynamic Electrochemistry at the Interface between Two Immiscible Electrolytes. *Electrochim. Acta* **2012**, *84*, 21–28. https://doi.org/10.1016/j.electacta.2012.03.118.

(8) Poltorak, L.; Eggink, I.; Hoitink, M.; Sudhölter, E. J. R.; De Puit, M. Electrified Soft Interface as a Selective Sensor for Cocaine Detection in Street Samples. *Anal. Chem.* **2018**, *90* (12), 7428–7433. https://doi.org/10.1021/acs.analchem.8b00916.

(9) Fantini, S.; Clohessy, J.; Gorgy, K.; Fusalba, F.; Johans, C.; Kontturi, K.; Cunnane, V. J. Influence of the Presence of a Gel in the Water Phase on the Electrochemical Transfer of Ionic Forms of β-Blockers across a Large Water|1,2-Dichloroethane Interface. *Eur. J. Pharm. Sci.* **2003**, *18* (3–4), 251–257. https://doi.org/10.1016/S0928-0987(03)00018-6.

(10) Collins, C. J.; Arrigan, D. W. M. Ion-Transfer Voltammetric Determination of the β-Blocker Propranolol in a Physiological Matrix at Silicon Membrane-Based Liquid|Liquid Microinterface Arrays. *Anal. Chem.* **2009**, *81* (6), 2344–2349. https://doi.org/10.1021/ac802644g.

(11) Liu, Y.; Strutwolf, J.; Arrigan, D. W. M. Ion-Transfer Voltammetric Behavior of Propranolol at Nanoscale Liquid-Liquid Interface Arrays. *Anal. Chem.* **2015**, *87* (8), 4487–4494. https://doi.org/10.1021/acs.analchem.5b00461.

(12) Huang, X.; Xie, L.; Lin, X.; Su, B. Detection of Metoprolol in Human Biofluids and Pharmaceuticals via Ion-Transfer Voltammetry at the Nanoscopic Liquid/Liquid Interface Array. *Anal. Chem.* **2017**, *89* (1), 945–951. https://doi.org/10.1021/acs.analchem.6b04099.

(13) Ribeiro, J. A.; Silva, F.; Pereira, C. M. Electrochemical Study of the Anticancer Drug Daunorubicin at a Water/Oil Interface: Drug Lipophilicity and Quantification. *Anal. Chem.* **2013**, *85* (3), 1582–1590. https://doi.org/10.1021/ac3028245.

(14) Kim, H. R.; Pereira, C. M.; Han, H. Y.; Lee, H. J. Voltammetric Studies of Topotecan Transfer across Liquid/Liquid Interfaces and Sensing Applications. *Anal. Chem.* **2015**, *87* (10), 5356–5362. https://doi.org/10.1021/acs.analchem.5b00653.

(15) Puri, S. R.; Kim, J. Kinetics of Antimicrobial Drug Ion Transfer at a Water/Oil Interface Studied by Nanopipet Voltammetry. *Anal. Chem.* **2019**, *91* (3), 1873–1879. https://doi.org/10.1021/acs.analchem.8b03593.

(16) Rudnicki, K.; Poltorak, L.; Skrzypek, S.; Sudhölter, E. J. R. Ion Transfer Voltammetry for Analytical Screening of Fluoroquinolone Antibiotics at the Water – 1.2-Dichloroethane Interface. *Anal. Chim. Acta* **2019**, *1085*, 75–84. https://doi.org/10.1016/j.aca.2019.07.065.

(17) Colombo, M. L.; McNeil, S.; Iwai, N.; Chang, A.; Shen, M. Electrochemical Detection of Dopamine via Assisted Ion Transfer at Nanopipet Electrode Using Cyclic Voltammetry. *J. Electrochem. Soc.* **2016**, *163* (4), H3072–H3076. https://doi.org/10.1149/2.0091604jes.

(18) Chen, R.; Yang, A.; Chang, A.; Oweimrin, P. F.; Romero, J.; Vichitcharoenpaisarn, P.; Tapia, S.; Ha, K.; Villaflor, C.; Shen, M. A Newly Synthesized Tris(Crown Ether) Ionophore for Assisted Ion Transfer at NanoITIES Electrodes. *ChemElectroChem* **2020**, *7* (4), 967–974. https://doi.org/10.1002/celc.201901997.

(19) Arrigan, D. W. M.; Ghita, M.; Beni, V. Selective Voltammetric Detection of Dopamine in the Presence of Ascorbate. *Chem. Commun.* **2004**, *4* (6), 732–733. https://doi.org/10.1039/b316493d.

(20) Zhan, D.; Mao, S.; Zhao, Q.; Chen, Z.; Hu, H.; Jing, P.; Zhang, M.; Zhu, Z.; Shao, Y. Electrochemical Investigation of Dopamine at the Water/1,2-Dichloroethane Interface. *Anal. Chem.* **2004**, *76* (14), 4128–4136. https://doi.org/10.1021/ac035339t.

(21) Beni, V.; Ghita, M.; Arrigan, D. W. M. Cyclic and Pulse Voltammetric Study of Dopamine at the Interface between Two Immiscible Electrolyte Solutions. *Biosens. Bioelectron.* **2005**, *20* (10 SPEC. ISS.), 2097–2103. https://doi.org/10.1016/j.bios.2004.08.004.

(22) Shen, M.; Qu, Z.; Deslaurier, J.; Welle, T. M.; Sweedler, J. V.; Chen, R. Single Synaptic Observation of Cholinergic Neurotransmission on Living Neurons: Concentration and Dynamics. *J. Am. Chem. Soc.* **2018**, *140* (25), 7764–7768. https://doi.org/10.1021/jacs.8b01989.

(23) Zdenek Samec, V. M. Electrolysis At The Interface Between Two Immiscible Electrolyte Solutions : Determination Of Acetylcholine By Differential Pulse Stripping Voltammetry. *Anal. Lett.* **1981**, *14* (15), 1241–1253. https://doi.org/10.1080/00032718108081455.

(24) Shao, Y.; Girault, H. H. Kinetics of the Transfer of Acetylcholine across the Water + Sucrose/ 1,2-Dichloroethane Interface. A Comparison between Ion Transport and Ion Transfer. *J. Electroanal. Chem.* **1990**, *282* (1–2), 59–72. https://doi.org/10.1016/0022-0728(91)85090-C.

(25) Shao, Y.; Liu, B.; Mirkin, M. V. Studying Ionic Reactions by a New Generation/Collection Technique. *J. Am. Chem. Soc.* **1998**, *120* (48), 12700–12701. https://doi.org/10.1021/ja983154b.

(26) Colombo, M. L.; Sweedler, J. V.; Shen, M. Nanopipet-Based Liquid-Liquid Interface Probes for the Electrochemical Detection of Acetylcholine, Tryptamine, and Serotonin via Ionic Transfer. *Anal. Chem.* **2015**, *87* (10), 5095–5100. https://doi.org/10.1021/ac504151e.

(27) Iwai, N. T.; Kramaric, M.; Crabbe, D.; Wei, Y.; Chen, R.; Shen, M. GABA Detection with Nano-ITIES Pipet Electrode: A New Mechanism, Water/DCE-Octanoic Acid Interface. *Anal. Chem.* **2018**, *90* (5), 3067–3072. https://doi.org/10.1021/acs.analchem.7b03099.

(28) Burgoyne, E. D.; Stockmann, T. J.; Molina-Osorio, A. F.; Shanahan, R.; McGlacken, G. P.; Scanlon, M. D. Electrochemical Detection of Pseudomonas Aeruginosa Quorum Sensing Molecules at a Liquid|Liquid Interface. *J. Phys. Chem. C* **2019**, *123* (40), 24643–24650. https://doi.org/10.1021/acs.jpcc.9b08350.

(29) Lagger, G.; Tomaszewski, L.; Osborne, M. D.; Seddon, B. J.; Girault, H. H. Electrochemical Extraction of Heavy Metal Ions Assisted by Cyclic Thioether Ligands. *J. Electroanal. Chem.* **1998**, *451* (1–2), 29–37. https://doi.org/10.1016/S0022-0728(97)00389-6.

(30) Wilke, S.; Wang, H.; Muraczewska, M.; Müller, H. Amperometric Detection of Heavy Metal Ions in Ion Pair Chromatography at an Array of Water/Nitrobenzene Micro Interfaces. *Fresenius. J. Anal. Chem.* **1996**, *356* (3–4), 233–236. https://doi.org/10.1007/s0021663560233.

(31) Mastouri, A.; Peulon, S.; Farcage, D.; Bellakhal, N.; Chaussé, A. Perfect Additivity of Microinterface Arrays for Liquid-Liquid Measurements: Application to Cadmium Ions Quantification. *Electrochim. Acta* **2014**, *120*, 212–218. https://doi.org/10.1016/j.electacta.2013.12.034.

(32) Mastouri, A.; Peulon, S.; Bellakhal, N.; Chaussé, A. M(II) Transfer across a Liquid-Liquid Microinterface Facilitated by a Complex Formation with 8-Hydroxyquinoline: Application to Quantification of Pb(II), Cd(II) and Zn(II) Alone or in Mixture in Effluents. *Electrochim. Acta* **2014**, *130*, 818–825. https://doi.org/10.1016/j.electacta.2014.03.073.

(33) Benvidi, A.; Lanjwani, S. N.; Ding, Z. Cd2+ Transfer across Water/1,2-Dichloroethane Microinterfaces Facilitated by Complex Formation with 1,10-Phenanthroline. *Electrochim. Acta* **2010**, *55* (6), 2196–2200. https://doi.org/10.1016/j.electacta.2009.11.056.

(34) Bingol, H.; Atalay, T. Interfacial Transfer of Cd2+ Assisted by 4′ - Morpholino-Acetophenone-4-Phenyl-3-Thiosemicarbazone across the Water/1,2-Dichloroethane Interface. *Cent. Eur. J. Chem.* **2010**, *8* (5), 1134–1139. https://doi.org/10.2478/s11532-010-0089-9.

(35) Lee, H. J.; Lagger, G.; Pereira, C. M.; Silva, A. F.; Girault, H. H. Amperometric Tape Ion Sensors for Cadmium(II) Ion Analysis. *Talanta* **2009**, *78* (1), 66–70. https://doi.org/10.1016/j.talanta.2008.10.059.

(36) Hossain, M. M.; Lee, S. H.; Girault, H. H.; Devaud, V.; Lee, H. J. Voltammetric Studies of Hexachromic Anion Transfer Reactions across Micro-Water/Polyvinylchloride-2-Nitrophenyloctylether Gel Interfaces for Sensing Applications. *Electrochim. Acta* **2012**, *82*, 12–18. https://doi.org/10.1016/j.electacta.2012.03.127.

(37) O'Mahony, A. M.; Scanlon, M. D.; Berduque, A.; Beni, V.; Arrigan, D. W. M.; Faggi, E.; Bencini, A. Voltammetry of Chromium(VI) at the Liquid|liquid Interface. *Electrochem. commun.* **2005**, *7* (10), 976–982. https://doi.org/10.1016/j.elecom.2005.06.011.

(38) Arrigan, D. W. M.; Hackett, M. J.; Mancera, R. L. Electrochemistry of Proteins at the Interface between Two Immiscible Electrolyte Solutions. *Curr. Opin. Electrochem.* **2018**, *12*, 27–32. https://doi.org/10.1016/j.coelec.2018.07.012.

(39) Arrigan, D. W. M.; Liu, Y. Electroanalytical Ventures at Nanoscale Interfaces Between Immiscible Liquids. *Annu. Rev. Anal. Chem.* **2016**, *9* (1), 145–161. https://doi.org/10.1146/annurev-anchem-071015-041415.

(40) Arrigan, D. W. M.; Alvarez de Eulate, E.; Liu, Y. Electroanalytical Opportunities Derived from Ion Transfer at Interfaces between Immiscible Electrolyte Solutions. *Aust. J. Chem.* **2016**, *69* (9), 1016–1032. https://doi.org/10.1071/CH15796.

(41) Arrigan, D.; Herzog, G.; Scanlon, M.; Strutwolf, J. Bioanalytical Applications of Electrochemistry at Liquid-Liquid Microinterfaces. In *Electroanalytical Chemistry : A Series of Advances*; 2013; pp 105–178. https://doi.org/10.1201/b15576-4.

(42) Sanchez Vallejo, L. J.; Ovejero, J. M.; Fernández, R. A.; Dassie, S. A. Simple Ion Transfer at Liquid|Liquid Interfaces. *Int. J. Electrochem.* **2012**, *2012*, 1–34. https://doi.org/10.1155/2012/462197.

(43) Herzog, G. Recent Developments in Electrochemistry at the Interface between Two Immiscible Electrolyte Solutions for Ion Sensing. *Analyst* **2015**, *140* (12), 3888–3896. https://doi.org/10.1039/c5an00601e.

(44) Goh, E.; Lee, H. J. Applications of Electrochemistry at Liquid/Liquid Interfaces for Ionizable Drug Molecule Sensing. *Rev. Polarogr.* **2016**, *62* (2+3), 77–84. https://doi.org/10.5189/revpolarography.62.77.

(45) Shen, M.; Colombo, M. L. Electrochemical Nanoprobes for the Chemical Detection of Neurotransmitters. *Anal. Methods* **2015**, *7* (17), 7095–7105. https://doi.org/10.1039/c5ay00512d.

(46) Sisk, G. D.; Herzog, G.; Glennon, J. D.; Arrigan, D. W. M. Assessment of Ion Transfer Amperometry at Liquid-Liquid Interfaces for Detection in CE. *Electrophoresis* **2009**, *30* (19), 3366–3371. https://doi.org/10.1002/elps.200900285.

(47) Ortuño, J. A.; Hernández, J.; Sánchez-Pedreño, C. Flow-Injection Amperometric Detection with Solvent Polymeric Membrane Ion Sensors. *Electroanalysis* **2004**, *16* (10), 827–831. https://doi.org/10.1002/elan.200302886.

(48) Pereira, C. M.; Oliveira, J. M.; Silva, R. M.; Silva, F. Amperometric Glucose Biosensor Based on Assisted Ion Transfer through Gel-Supported Microinterfaces. *Anal. Chem.* **2004**, *76* (18), 5547–5551. https://doi.org/10.1021/ac0498765.

(49) Berduque, A.; Arrigan, D. W. M. Selectivity in the Coextraction of Cation and Anion by Electrochemically Modulated Liquid-Liquid Extraction. *Anal. Chem.* **2006**, *78* (8), 2717–2725. https://doi.org/10.1021/ac0521192.

(50) Deryabina, M. A.; Hansen, S. H.; Jensen, H. Versatile Flow-Injection Amperometric Ion Detector Based on an Interface between Two Immiscible Electrolyte Solutions: Numerical and Experimental Characterization. *Anal. Chem.* **2011**, *83* (19), 7388–7393. https://doi.org/10.1021/ac201387r.

(51) Berduque, A.; Sherburn, A.; Ghita, M.; Dryfe, R. A. W.; Arrigan, D. W. M. Electrochemically Modulated Liquid-Liquid Extraction of Ions. *Anal. Chem.* **2005**, *77* (22), 7310–7318. https://doi.org/10.1021/ac051029u.

(52) Scanlon, M. D.; Berduque, A.; Strutwolf, J.; Arrigan, D. W. M. Flow-Injection Amperometry at Microfabricated Silicon-Based μ-Liquid-Liquid Interface Arrays. *Electrochim. Acta* **2010**, *55* (14). https://doi.org/10.1016/j.electacta.2008.12.014.

(53) Poltorak, L.; Sudhölter, E. J. R.; de Puit, M. Electrochemical Cocaine (Bio)Sensing. From Solid Electrodes to Soft Junctions. *TrAC - Trends Anal. Chem.* **2019**, *114*, 48–55. https://doi.org/10.1016/j.trac.2019.02.025.

(54) Velázquez-Manzanares, M.; Martínez, H. G.; Yudi, L. M.; Amador-Hernández, J.; de la Garza Rodríguez, I. M.; Urbina, E. M. C. Electrochemical Behavior of Simetryn Herbicide at Water|1,2-Dichloroethane Interface. *J. Electrochem. Soc.* **2019**, *166* (8), H286–H290. https://doi.org/10.1149/2.0481908jes.

(55) Olmos, J. M.; Pereira, C. M. Electrochemical Sensing and Characterization of Denatonium Ion by Ion Transfer at Polarized Liquid/Liquid Interfaces. *J. Electroanal. Chem.* **2020**, *859*, 1–5. https://doi.org/10.1016/j.jelechem.2020.113860.

(56) Berduque, A.; Zazpe, R.; Arrigan, D. W. M. Electrochemical Detection of Dopamine Using Arrays of Liquid-Liquid Micro-Interfaces Created within Micromachined Silicon Membranes. *Anal. Chim. Acta* **2008**, *611* (2), 156–162. https://doi.org/10.1016/j.aca.2008.01.077.

(57) Molina, A.; Serna, C.; Ortuño, J. A.; Gonzalez, J.; Torralba, E.; Gil, A. Differential Pulse Voltammetry for Ion Transfer at Liquid Membranes with Two Polarized Interfaces. *Anal. Chem.* **2009**, *81* (11), 4220–4225. https://doi.org/10.1021/ac802503b.

(58) Yufei, C.; Cunnane, V. J.; Schiffrin, D. J.; Mutomäki, L.; Kontturi, K. Interfacial Capacitance and Ionic Association at Electrified Liquid/Liquid Interfaces. *J. Chem. Soc., Faraday Trans.* **1991**, *87* (1), 107–114. https://doi.org/10.1039/FT9918700107.

(59) Suárez-Herrera, M. F.; Scanlon, M. D. On the Non-Ideal Behaviour of Polarised Liquid-Liquid Interfaces. *Electrochim. Acta* **2019**, *328*, 135110. https://doi.org/10.1016/j.electacta.2019.135110.

(60) Strutwolf, J.; Scanlon, M. D.; Arrigan, D. W. M. The Performance of Differential Pulse Stripping Voltammetry at Micro-Liquid-Liquid Interface Arrays. *J. Electroanal. Chem.* **2010**, *641* (1–2), 7–13. https://doi.org/10.1016/j.jelechem.2010.01.020.

(61) Scanlon, M. D.; Strutwolf, J.; Blake, A.; Iacopino, D.; Quinn, A. J.; Arrigan, D. W. M. Ion-Transfer Electrochemistry at Arrays of Nanointerfaces between Immiscible Electrolyte Solutions Confined within Silicon Nitride Nanopore Membranes. *Anal. Chem.* **2010**, *82* (14), 6115–6123. https://doi.org/10.1021/ac1008282.

(62) Scanlon, M. D.; Arrigan, D. W. M. Enhanced Electroanalytical Sensitivity via Interface Miniaturisation: Ion Transfer Voltammetry at an Array of Nanometre Liquid-Liquid Interfaces. *Electroanalysis* **2011**, *23* (4), 1023–1028. https://doi.org/10.1002/elan.201000667.

(63) Vazquez, P.; Herzog, G.; O'Mahony, C.; O'Brien, J.; Scully, J.; Blake, A.; O'Mathuna, C.; Galvin, P. Microscopic Gel-Liquid Interfaces Supported by Hollow Microneedle Array for Voltammetric Drug Detection. *Sensors Actuators, B Chem.* **2014**, *201*, 572–578. https://doi.org/10.1016/j.snb.2014.04.080.

(64) Sairi, M.; Arrigan, D. W. M. Electrochemical Detection of Ractopamine at Arrays of Micro-Liquid | Liquid Interfaces. *Talanta* **2015**, *132* (15), 205–214. https://doi.org/10.1016/j.talanta.2014.08.060.

(65) Jeshycka, S.; Han, H. Y.; Lee, H. J. Voltammetric Understanding of Ionizable Doxorubicin Transfer Reactions across Liquid/Liquid Interfaces and Sensor Development. *Electrochim. Acta* **2017**, *245*, 211–218. https://doi.org/10.1016/j.electacta.2017.05.096.

(66) Izadyar, A. Stripping Voltammetry at the Interface between Two Immiscible Electrolyte Solutions: A Review Paper. *Electroanalysis* **2018**, *30* (10), 2210–2221. https://doi.org/10.1002/elan.201800279.

(67) Herzog, G.; Moujahid, W.; Strutwolf, J.; Arrigan, D. W. M. Interactions of Proteins with Small Ionised Molecules: Electrochemical Adsorption and Facilitated Ion Transfer Voltammetry of Haemoglobin at the Liquidliquid Interface. *Analyst* **2009**, *134* (8), 1608–1613. https://doi.org/10.1039/b905441n.

(68) Thomsen, A. E.; Jensen, H.; Jorgensen, L.; van de Weert, M.; Østergaard, J. Studies on Human Insulin Adsorption Kinetics at an Organic-Aqueous Interface Determined Using a Label-Free Electroanalytical Approach. *Colloids Surfaces B Biointerfaces* **2008**, *63* (2), 243–248. https://doi.org/10.1016/j.colsurfb.2007.12.005.

(69) Smirnov, E.; Peljo, P.; Scanlon, M. D.; Girault, H. H. Gold Nanofilm Redox Catalysis for Oxygen Reduction at Soft Interfaces. *Electrochim. Acta* **2016**, *197*, 362–373. https://doi.org/10.1016/j.electacta.2015.10.104.

(70) Wandlowski, T.; Mareček, V.; Samec, Z. Galvani Potential Scales for Water-Nitrobenzene and Water-1,2-Dichloroethane Interfaces. *Electrochim. Acta* **1990**, *35* (7), 1173–1175. https://doi.org/10.1016/0013-4686(90)80035-M.

(71) Bard, A. J.; Faulkner, L. R. Chapter 10: Techniques Based on Concepts of Impedance. In *Electrochemical Methods, Fundamentals and Applications*; John Wiley & Sons, Inc, 2001; pp 368–416.

(72) He, P.; Faulkner, L. R. Intelligent, Automatic Compensation of Solution Resistance. *Anal. Chem.* **1986**, *58* (3), 517–523. https://doi.org/10.1021/ac00294a004.

(73) Wandlowski, T.; Mareček, V.; Samec, Z. Kinetic Analysis of the Picrate Ion Transfer across the Interface between Two Immiscible Electrolyte Solutions from Impedance Measurements at the Equilibrium Potential. *J. Electroanal. Chem.* **1988**, *242* (1–2), 291–302. https://doi.org/10.1016/0022-0728(88)80258-4.

(74) Wandlowski, T.; Mareček, V.; Holub, K.; Samec, Z. Ion Transfer across Liquid-Liquid Phase Boundaries: Electrochemical Kinetics by Faradaic Impedance. *J. Phys. Chem.* **1989**, *93* (25), 8204–8212. https://doi.org/10.1021/j100362a013.

(75) Poltorak, L.; Sudhölter, E. J. R.; de Smet, L. C. P. M. Effect of Charge of Quaternary Ammonium Cations on Lipophilicity and Electroanalytical Parameters: Task for Ion Transfer

Voltammetry. *J. Electroanal. Chem.* **2017**, *796* (April), 66–74. https://doi.org/10.1016/j.jelechem.2017.04.051.

(76) Rodríguez-López, J.; Videa, M. Study of the Ion Transfer of Quaternary Ammonium Ions by SWV. *J. Mex. Chem. Soc.* **2012**, *56* (4), 417–425.

(77) Wandlowski, T.; Mareček, V.; Samec, Z.; Fuoco, R. Effect of Temperature on the Ion Transfer across an Interface between Two Immiscible Electrolyte Solutions: Ion Transfer Dynamics. *J. Electroanal. Chem.* **1992**, *331* (1–2), 765–782. https://doi.org/10.1016/0022-0728(92)85005-N.

(78) Aminur Rahman, M.; Doe, H. Ion Transfer of Tetraalkylammonium Cations at an Interface between Frozen Aqueous Solution and 1,2-Dichloroethane. *J. Electroanal. Chem.* **1997**, *424* (1–2), 159–164. https://doi.org/10.1016/S0022-0728(96)04906-6.

(79) Dabir S. Viswanath; Ghosh, T. K.; Prasad, D. H. L.; Dutt, N. V. K.; Rani, K. Y. *Viscosity of Liquids: Theory, Estimation, Experiment, and Data*; Springer: Dordrecht, The Netherlands, 2007.

(80) Sladkov, V.; Guillou, V.; Peulon, S.; L'Her, M. Voltammetry of Tetraalkylammonium Picrates at Water|nitrobenzene and Water|dichloroethane Microinterfaces; Influence of Partition Phenomena. *J. Electroanal. Chem.* **2004**, *573* (1), 129–138. https://doi.org/10.1016/j.jelechem.2004.06.027.

(81) Bard, A. J.; Faulkner, L. R. Electroactive Layers and Modified Electrodes. In *Electrochemical methods: fundamentals and applications*; John Wiley & Sons, Inc, 2001; pp 580–631.

(82) Lhotský, A.; Mareček, V.; Záliš, S.; Samec, Z. Specific Adsorption of Tetraalkylammonium Cations at the Water|1,2-Dichloroethane Interface Revisited. *J. Electroanal. Chem.* **2005**, *585* (2), 269–274. https://doi.org/10.1016/j.jelechem.2005.07.026.

(83) Nishi, N.; Izawa, K.; Yamamoto, M.; Kakiuchi, T. AC-Modulated Voltfluorometric Study of the Transient Adsorption of Rose Bengal Dianions in the Transfer across the 1,2-Dichloroethane|water Interface. *J. Phys. Chem. B* **2001**, *105* (34), 8162–8169. https://doi.org/10.1021/jp010875f.

(84) Nishi, N.; Kakiuchi, T. Potential-Dependent Adsorption of Transferring Ions Having Asymmetric Charge Distribution at the 1,2-Dichloroethane|Water Interface and Its Ion-

Transfer Kinetics Studied by AC-Modulated Voltfluorometry. *Russ. J. Electrochem.* **2003**, *39* (2), 125–129. https://doi.org/10.1023/A:1022396522597.

(85) Olaya, A. J.; Ge, P.; Girault, H. H. Ion Transfer across the Water|trifluorotoluene Interface. *Electrochem. commun.* **2012**, *19* (1), 101–104. https://doi.org/10.1016/j.elecom.2012.03.010.

(86) Scheu, R.; Chen, Y.; Subinya, M.; Roke, S. Stern Layer Formation Induced by Hydrophobic Interactions: A Molecular Level Study. *J. Am. Chem. Soc.* **2013**, *135* (51), 19330–19335. https://doi.org/10.1021/ja4102858.

(87) Herzog, G.; Arrigan, D. W. M. Determination of Trace Metals by Underpotential Deposition-Stripping Voltammetry at Solid Electrodes. *TrAC - Trends Anal. Chem.* **2005**, *24*, 208–217. https://doi.org/10.1016/j.trac.2004.11.014.

(88) Bonfil, Y.; Brand, M.; Kirowa-Eisner, E. Trace Determination of Mercury by Anodic Stripping Voltammetry at the Rotating Gold Electrode. *Anal. Chim. Acta* **2000**, *424* (1), 65–76. https://doi.org/10.1016/S0003-2670(00)01074-6.

(89) Bonfil, Y.; Brand, M.; Kirowa-Eisner, E. Characteristics of Subtractive Anodic Stripping Voltammetry of Pb and Cd at Silver and Gold Electrodes. *Anal. Chim. Acta* **2002**, *464* (1), 99–114. https://doi.org/10.1016/S0003-2670(02)00489-0.

(90) Bonfil, Y.; Kirowa-Eisner, E. Determination of Nanomolar Concentrations of Lead and Cadmium by Anodic-Stripping Voltammetry at the Silver Electrode. *Anal. Chim. Acta* **2002**, *457* (2), 285–296. https://doi.org/10.1016/S0003-2670(02)00016-8.

(91) Bonfil, Y.; Brand, M.; Kirowa-Eisner, E. Characteristics of Subtractive Anodic Stripping Voltammetry of Lead, Cadmium and Thallium at Silver-Gold Alloy Electrodes. *Electroanalysis* **2003**, *15* (17), 1369–1376. https://doi.org/10.1002/elan.200302739.

Table of Contents artwork